Corneal biometry from volumetric SDOCT and comparison with existing clinical modalities

Anthony N. Kuo,[1,*] Ryan P. McNabb,[2] Mingtao Zhao,[2] Francesco LaRocca,[2] Sandra S. Stinnett,[1,3] Sina Farsiu,[1,2] and Joseph A. Izatt[2,1]

[1]*Department of Ophthalmology, Duke University Medical Center, Durham NC 27710, USA*
[2]*Department of Biomedical Engineering, Duke University, 136 Hudson Hall, Box 90281, Durham NC 27708, USA*
[3]*Department of Biostatistics and Bioinformatics, Duke University Medical Center, Durham NC 27710, USA*
*anthony.kuo@duke.edu

Abstract: We present a comparison of corneal biometric values from dense volumetric spectral domain optical coherence tomography (SDOCT) scans to reference values in both phantoms and clinical subjects. We also present a new optically based "keratometric equivalent power" formula for SDOCT that eliminates previously described discrepancies between corneal power form SDOCT and existing clinical modalities. Phantom objects of varying radii of curvature and corneas of normal subjects were imaged with a clinical SDOCT system. The optically corrected three-dimensional surfaces were used to recover radii of curvature and power as appropriate. These were then compared to the manufacturer's reference values in phantoms and to measurements from topography and Scheimpflug photography in subjects. In phantom objects, paired differences between SDOCT and reference values for radii of curvature were not statistically significant. In subjects, there were no significant paired differences between SDOCT and reference values from the other modalities for anterior radius and corneal keratometric power. In contrast to other studies, we found that dense volumetric scans with available SDOCT can be used to recover corneal biometric values—including power—that correspond well with existing clinical measurements.

© 2012 Optical Society of America

OCIS codes: (170.4500) Optical coherence tomography; (170.4470) Ophthalmology; (170.4460) Ophthalmic optics and devices.

References and links

1. T. Olsen, "On the calculation of power from curvature of the cornea," Br. J. Ophthalmol. **70**(2), 152–154 (1986).
2. E. Hecht, *Optics* (Addison Wesley, New York, NY, 2002).
3. J. Schwiegerling, *Field Guide to Visual and Ophthalmic Optics* (SPIE Press, Bellingham, WA, 2004).
4. B. Seitz, A. Langenbucher, N. X. Nguyen, M. M. Kus, and M. Küchle, "Underestimation of intraocular lens power for cataract surgery after myopic photorefractive keratectomy," Ophthalmology **106**(4), 693–702 (1999).
5. D. Huang, E. A. Swanson, C. P. Lin, J. S. Schuman, W. G. Stinson, W. Chang, M. R. Hee, T. Flotte, K. Gregory, C. A. Puliafito, and J. G. Fujimoto, "Optical coherence tomography," Science **254**(5035), 1178–1181 (1991).
6. E. A. Swanson, J. A. Izatt, M. R. Hee, D. Huang, C. P. Lin, J. S. Schuman, C. A. Puliafito, and J. G. Fujimoto, "In vivo retinal imaging by optical coherence tomography," Opt. Lett. **18**(21), 1864–1866 (1993).
7. J. A. Izatt, M. R. Hee, E. A. Swanson, C. P. Lin, D. Huang, J. S. Schuman, C. A. Puliafito, and J. G. Fujimoto, "Micrometer-scale resolution imaging of the anterior eye in vivo with optical coherence tomography," Arch. Ophthalmol. **112**(12), 1584–1589 (1994).
8. M. Wojtkowski, R. Leitgeb, A. Kowalczyk, T. Bajraszewski, and A. F. Fercher, "In vivo human retinal imaging by Fourier domain optical coherence tomography," J. Biomed. Opt. **7**(3), 457–463 (2002).
9. K. Bizheva, N. Hutchings, L. Sorbara, A. A. Moayed, and T. Simpson, "In vivo volumetric imaging of the human corneo-scleral limbus with spectral domain OCT," Biomed. Opt. Express **2**(7), 1794–1802 (2011).
10. M. L. Gabriele, G. Wollstein, H. Ishikawa, L. Kagemann, J. Xu, L. S. Folio, and J. S. Schuman, "Optical coherence tomography: history, current status, and laboratory work," Invest. Ophthalmol. Vis. Sci. **52**(5), 2425–2436 (2011).

11. M. Tang, Y. Li, M. Avila, and D. Huang, "Measuring total corneal power before and after laser in situ keratomileusis with high-speed optical coherence tomography," J. Cataract Refract. Surg. **32**(11), 1843–1850 (2006).
12. M. Tang, A. Chen, Y. Li, and D. Huang, "Corneal power measurement with Fourier-domain optical coherence tomography," J. Cataract Refract. Surg. **36**(12), 2115–2122 (2010).
13. M. Gora, K. Karnowski, M. Szkulmowski, B. J. Kaluzny, R. Huber, A. Kowalczyk, and M. Wojtkowski, "Ultra high-speed swept source OCT imaging of the anterior segment of human eye at 200 kHz with adjustable imaging range," Opt. Express **17**(17), 14880–14894 (2009).
14. K. Karnowski, B. J. Kaluzny, M. Szkulmowski, M. Gora, and M. Wojtkowski, "Corneal topography with high-speed swept source OCT in clinical examination," Biomed. Opt. Express **2**(9), 2709–2720 (2011).
15. F. LaRocca, S. J. Chiu, R. P. McNabb, A. N. Kuo, J. A. Izatt, and S. Farsiu, "Robust automatic segmentation of corneal layer boundaries in SDOCT images using graph theory and dynamic programming," Biomed. Opt. Express **2**(6), 1524–1538 (2011).
16. M. Zhao, A. N. Kuo, and J. A. Izatt, "3D refraction correction and extraction of clinical parameters from spectral domain optical coherence tomography of the cornea," Opt. Express **18**(9), 8923–8936 (2010).
17. S. Ortiz, D. Siedlecki, I. Grulkowski, L. Remon, D. Pascual, M. Wojtkowski, and S. Marcos, "Optical distortion correction in optical coherence tomography for quantitative ocular anterior segment by three-dimensional imaging," Opt. Express **18**(3), 2782–2796 (2010).
18. R. C. Lin, M. A. Shure, A. M. Rollins, J. A. Izatt, and D. Huang, "Group index of the human cornea at 1.3-microm wavelength obtained in vitro by optical coherence domain reflectometry," Opt. Lett. **29**(1), 83–85 (2004).
19. D. Malacara and Z. Malacara, *Handbook of Optical Design* (Marcel Dekker, New York, NY, 2004).
20. V. A. Sicam, M. Dubbelman, and R. G. van der Heijde, "Spherical aberration of the anterior and posterior surfaces of the human cornea," J. Opt. Soc. Am. A **23**(3), 544–549 (2006).
21. D. A. Atchison and G. Smith, *Optics of the Human Eye* (Butterworth-Heinemann, Boston, MA, 2002).
22. N. E. Norrby, "Unfortunate discrepancies," J. Cataract Refract. Surg. **24**(4), 433–434 (1998).
23. F. A. Jenkins and H. E. White, *Fundamentals of Optics* (McGraw-Hill, New York, NY, 1950).
24. J. M. Bland and D. G. Altman, "Statistical methods for assessing agreement between two methods of clinical measurement," Lancet **327**(8476), 307–310 (1986).
25. B. Efron and R. J. Tibshirani, *An Introduction to the Bootstrap* (Chapman & Hall/CRC, Washington, D.C., 1993).
26. L. Wang, A. M. Mahmoud, B. L. Anderson, D. D. Koch, and C. J. Roberts, "Total corneal power estimation: ray tracing method versus gaussian optics formula," Invest. Ophthalmol. Vis. Sci. **52**(3), 1716–1722 (2011).
27. J. D. Ho, C. Y. Tsai, R. J. Tsai, L. L. Kuo, I. L. Tsai, and S. W. Liou, "Validity of the keratometric index: evaluation by the Pentacam rotating Scheimpflug camera," J. Cataract Refract. Surg. **34**(1), 137–145 (2008).
28. J. T. Holladay, W. E. Hill, and A. Steinmueller, "Corneal power measurements using scheimpflug imaging in eyes with prior corneal refractive surgery," J. Refract. Surg. **25**(10), 862–868 (2009).
29. M. Dubbelman, H. A. Weeber, R. G. van der Heijde, and H. J. Völker-Dieben, "Radius and asphericity of the posterior corneal surface determined by corrected Scheimpflug photography," Acta Ophthalmol. Scand. **80**(4), 379–383 (2002).
30. J. M. Royston, M. C. Dunne, and D. A. Barnes, "Measurement of the posterior corneal radius using slit lamp and Purkinje image techniques," Ophthalmic Physiol. Opt. **10**(4), 385–388 (1990).
31. R. F. Lowe and B. A. Clark, "Posterior corneal curvature. Correlations in normal eyes and in eyes involved with primary angle-closure glaucoma," Br. J. Ophthalmol. **57**(7), 464–470 (1973).
32. C. Edmund, "Posterior corneal curvature and its influence on corneal dioptric power," Acta Ophthalmol. (Copenh.) **72**(6), 715–720 (1994).
33. M. Doors, L. P. J. Cruysberg, T. T. J. M. Berendschot, J. Brabander, F. Verbakel, C. A. B. Webers, and R. M. M. A. Nuijts, "Comparison of central corneal thickness and anterior chamber depth measurements using three imaging technologies in normal eyes and after phakic intraocular lens implantation," Graefes Arch. Clin. Exp. Ophthalmol. **247**(8), 1139–1146 (2009).
34. S. Fukuda, K. Kawana, Y. Yasuno, and T. Oshika, "Anterior ocular biometry using 3-dimensional optical coherence tomography," Ophthalmology **116**(5), 882–889 (2009).
35. D. S. Grewal, G. S. Brar, and S. P. Grewal, "Assessment of central corneal thickness in normal, keratoconus, and post-laser in situ keratomileusis eyes using Scheimpflug imaging, spectral domain optical coherence tomography, and ultrasound pachymetry," J. Cataract Refract. Surg. **36**(6), 954–964 (2010).
36. C. M. Prospero Ponce, K. M. Rocha, S. D. Smith, and R. R. Krueger, "Central and peripheral corneal thickness measured with optical coherence tomography, Scheimpflug imaging, and ultrasound pachymetry in normal, keratoconus-suspect, and post-laser in situ keratomileusis eyes," J. Cataract Refract. Surg. **35**(6), 1055–1062 (2009).
37. S. Ortiz, D. Siedlecki, P. Pérez-Merino, N. Chia, A. de Castro, M. Szkulmowski, M. Wojtkowski, and S. Marcos, "Corneal topography from spectral optical coherence tomography (sOCT)," Biomed. Opt. Express **2**(12), 3232–3247 (2011).
38. B. Potsaid, B. Baumann, D. Huang, S. Barry, A. E. Cable, J. S. Schuman, J. S. Duker, and J. G. Fujimoto, "Ultrahigh speed 1050nm swept source/Fourier domain OCT retinal and anterior segment imaging at 100,000 to 400,000 axial scans per second," Opt. Express **18**(19), 20029–20048 (2010).

39. M. Shen, M. R. Wang, J. Wang, Y. Yuan, and F. Chen, "Entire contact lens imaged in vivo and in vitro with spectral domain optical coherence tomography," Eye Contact Lens **36**(2), 73–76 (2010).
40. A. M. Davis, M. A. Choma, and J. A. Izatt, "Heterodyne swept-source optical coherence tomography for complete complex conjugate ambiguity removal," J. Biomed. Opt. **10**(6), 064005 (2005).
41. B. Hofer, B. Povazay, B. Hermann, A. Unterhuber, G. Matz, and W. Drexler, "Dispersion encoded full range frequency domain optical coherence tomography," Opt. Express **17**(1), 7–24 (2009).
42. M. Yamanari, S. Makita, Y. Lim, and Y. Yasuno, "Full-range polarization-sensitive swept-source optical coherence tomography by simultaneous transversal and spectral modulation," Opt. Express **18**(13), 13964–13980 (2010).
43. A. H. Dhalla, D. Nankivil, and J. A. Izatt, "Complex conjugate resolved heterodyne swept source optical coherence tomography using coherence revival," Biomed. Opt. Express **3**(3), 633–649 (2012).
44. T. O. Salmon and L. N. Thibos, "Videokeratoscope-line-of-sight misalignment and its effect on measurements of corneal and internal ocular aberrations," J. Opt. Soc. Am. A **19**(4), 657–669 (2002).

1. Introduction

Measurement of corneal biometric values is a requisite for surgical alteration of ocular optical elements. Procedures such as cataract surgery—among the most common surgical procedures performed worldwide—are dependent on the ability to characterize the optical properties of the eye. In particular, measurement of the optical power of the cornea—representing two-thirds of the refractive power of the eye—is critical in achieving desired refractive results.

For the purposes of current clinical ophthalmic optics as is used in cataract surgery, the cornea is assumed to be a spherical refractive element, and the curvature of this element is then related to its refractive power via lens formulas [1,2]. Illuminated ring based platforms such as keratometry and topography have been in routine use for the measurement of corneal curvature and power in preparation for surgical procedures. However, keratometry and topography are only able to measure the curvature of the anterior corneal surface. To characterize the optical properties of the cornea as a whole, assumptions must be made regarding the curvature and power contribution from the unmeasured posterior corneal surface [3].

These assumptions are valid for routine use in *normal* eyes. However, when the cornea is surgically altered as in laser refractive surgery (LASIK, PRK, and others), these assumptions no longer hold true and the biometric values normally generated by these devices can lead to undesired, erroneous clinical outcomes [4]. There is a need then, to develop tomographic imaging technologies that can measure both the anterior and posterior surface curvatures without a fixed, assumed relationship between the two.

Optical coherence tomography (OCT) is a micrometer scale tomographic imaging modality that is in widespread use in ophthalmology [5–10] and could be used for measuring these corneal biometric values. Prior work with time-domain OCT implementations to determine corneal biometry showed promise but were thought to be compromised by motion errors due to the relatively slow sequential data acquisition rates with time-domain OCT [11].

Recent experiences with higher-speed, higher-resolution Fourier domain OCT implementations have been more successful but still noted a discrepancy of over a diopter between corneal power from OCT and existing clinical modalities [12]. Moreover, to minimize the acquisition time, reported spectral domain OCT (SDOCT) efforts have sampled the cornea less densely than found in other tomographic systems and have processed the acquired data primarily in two dimensional planes [12]; reported higher-speed swept-source OCT (SSOCT) efforts have required the use of dedicated research systems specialized for this particular application [13,14].

In this study, we describe the use of existing commercial SDOCT as is widely available in the ophthalmic community to densely sample the cornea volumetrically and to generate common corneal biometric values from the three-dimensional data sets. Furthermore, to ensure a clinically accurate reference for comparison, we chose to study a normal population where the keratometric assumptions made by standard clinical devices about the cornea should remain valid. This eliminated pathology or surgical alterations as confounding

variables and allowed us to directly determine the agreement of our SDOCT corneal biometric measurements with existing clinical modalities.

2. Methods

All OCT imaging in this study used a clinical retinal spectral domain OCT system (λ_0 = 859 nm; $\Delta\lambda$ = 53.9 nm; 6 µm axial optical resolution in air, 4.4 µm in tissue; 20 kHz A scan acquisition rate) configured for anterior segment imaging by using a telecentric focusing objective available from the manufacturer (Bioptigen, Research Triangle Park, NC).

Figure 1 briefly illustrates the sample imaging and post-processing procedure used. The scan protocol used volumes composed of 50 radial B-scans each with 1000 A-scans and 1024 pixel depth; at a 20 kHz rate, each volume was acquired in approximately 2.5 seconds. Each B-scan was nominally 6 mm in length. Radial scans were used to maximize the signal to noise ratio in the central region of each B-scan given the curvature of the cornea and the known phenomena of depth-dependent drop-off in SDOCT. Using 50 radial scans was comparable in scan density to that used in other clinical imaging devices such as the Pentacam (Oculus; Wetzler, Germany). Each scan was also centered on the saturation artifact. This artifact is the result of reflection from the apex of a curved surface, and this alignment technique allows for the placement of that apex at the center of the volume. The lateral and axial dimensions and telecentricity of the imaged sample space were characterized by imaging a flat dual-axis linear-scale stage micrometer (NT58-763; Edmund Optics; Barrington, NJ).
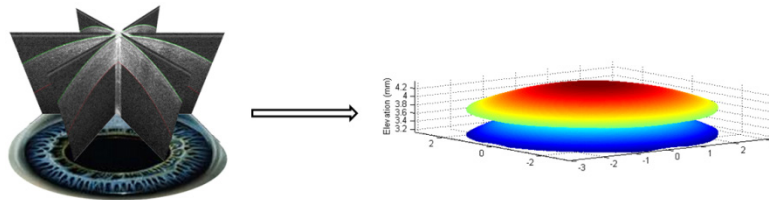

Fig. 1. **Acquisition and post-processing of volumetric corneal SDOCT data.** For each phantom and imaged eye, 50 radially oriented B-scans were captured. (Only 3 B-scans are shown in the figure for clarity). Each B-scan was then automatically segmented and corrected for optical artifacts in post-processing to generate the three-dimensional epithelial and endothelial surfaces. These surfaces were used to determine the corneal biometric measures (radii or curvature, power, and central thickness) for SDOCT.

Fully automated segmentation of the anterior and posterior corneal surfaces from the images was accomplished via dynamic programming based on graph theory [15]. Rudimentary axial motion correction was made by assuming that the scan axis of rotation was shared in all B-scans, and thus by registering the epithelial surface in the center A-scan of all B-scans within a volume. Removal of optical artifacts such as non-telecentricity and refraction in three-dimensions was accomplished using our previously published algorithms [16] (also described by Ortiz et al. [17]). Refractive indices of samples for three-dimensional refraction correction were provided by the manufacturer for the contact lens phantoms or determined experimentally for the cornea using previously reported techniques [18] which resulted in n_{cornea} = 1.387 for our SDOCT system source.

Anterior and posterior corneal curvature values were determined by least squares fitting of the optically-corrected three-dimensional corneal surfaces to the equation for a conicoid of revolution for a sphere [19,20]:

$$(z - z_0) = \frac{c\left((x - x_0)^2 + (y - y_0)^2\right)^2}{1 + \sqrt{1 - c^2\left((x - x_0)^2 + (y - y_0)^2\right)^2}} \tag{1}$$

Here c is the inverse of the radius of curvature, (x, y, z) are the surface points, and (x_0, y_0, z_0) is the vertex. Surface points within the central 5 mm in diameter zone were used for curvature fitting to exclude peripheral areas of low SNR due to SDOCT fall-off.

The paraxial corneal power (inverse front focal length) was then determined via the thick lens equation [1]:

$$\Phi = \frac{n_{cornea} - n_{air}}{r_{anterior}} + \frac{n_{aqueous} - n_{cornea}}{r_{posterior}} - \frac{CCT}{n_{cornea}} \cdot \frac{n_{cornea} - n_{air}}{r_{anterior}} \cdot \frac{n_{aqueous} - n_{cornea}}{r_{posterior}} \qquad (2)$$

Here, CCT is the central cornea thickness, the radii are the inverse curvatures from above, and the refractive indices are the Gullstrand values routinely found in the literature with $n_{cornea} = 1.376$, $n_{air} = 1.000$, and $n_{aqueous} = 1.336$ [21].

Because topography devices use a keratometric index (usually given as 1.3375), the rear focal point is actually referenced in these devices to the posterior vertex rather than the rear principal plane as in the paraxial lens formulas [22]. Hence, to also determine a "keratometric equivalent power" for SDOCT, we used the vertex power formula [23] with the appropriate ophthalmic variables:

$$\Phi_{KEP} = \frac{\Phi}{1 - \frac{CCT}{n_{cornea}} \cdot \frac{n_{cornea} - n_{air}}{r_{anterior}}} \qquad (3)$$

Additional detail regarding the scan protocol and post-processing algorithms can be found in Zhao et al. [16]. All post-processing algorithms were implemented and executed in MATLAB (MathWorks; Natick, MA). All statistical analyses were performed in MATLAB and SAS (Cary, NC).

2.1. Phantom validation

To ensure that the scanning protocol and post-processing algorithms produced valid curvature values, imaging of reference samples was undertaken. Two types of phantoms were used. First, three calibration spheres of varying curvature used for the calibration of a topography device were imaged. This represented the ability to image a curved surface in air such as in the case of the corneal epithelium.

Secondly, 6 rigid gas permeable lenses of varying known base curvatures (conformAthin; Conforma; Norfolk, VA) were each imaged in triplicate. This evaluated the ability to image a posterior curved surface after it had been refracted through an anterior curved surface and passed through some thickness of sample, as would be the case for the corneal endothelial surface. Each of the 6 contacts was placed convex (anterior) side towards the SDOCT onto a rubber grommet on a three-axis linear translation stage and each imaged once. This was then repeated for the group twice more. Each contact lens and the grommet were removed from the stage after each individual measurement. This resulted in volumetric data for 6 contact lenses, each imaged in triplicate, but with some random positional variability (triplicate measurements were not made by simply imaging the contact lens in the same position three times).

The nonparametric Wilcoxon signed rank test was performed to identify any significant differences from zero (with $\alpha = 0.05$) between the mean SDOCT measures and reference values.

2.2. Subject imaging

This portion of the study followed the tenets of the Declaration of Helsinki. Informed consent was obtained from the subjects after explanation of the nature and possible consequences of

the study. This research was approved by the Duke University Medical Center Institutional Review Board.

Healthy volunteers drawn from researchers and employees at our institution without known ocular pathology other than ametropia were asked to participate in subject imaging. Soft contact lens wearers were asked not to wear their contacts for at least 3 days prior to imaging; no subject wore rigid gas permeable lenses. Each subject was asked to fixate on a fixation target aligned with the optical axis of the SDOCT system, and the above described scan protocol was used to acquire three volumetric data sets of the subject's cornea. During the same session, each SDOCT imaged eye was also imaged with a topography device (Atlas 995; Carl Zeiss Meditec; Dublin, CA) and a Scheimpflug imaging device (Pentacam) for comparison. The SDOCT image data was post-processed as described above, and the anterior corneal curvature (r_a), posterior corneal curvature (r_p), corneal power (Φ, Φ_{KEP}), and central corneal thickness (CCT) for each imaged cornea were calculated. Comparable values from the topography device (r_a at (0,0) and mean simulated keratometry—SimK) and the Scheimpflug device (mean r_a, mean r_p, Equivalent K Reading—EKR, and CCT) were generated by each respective device's own proprietary, on-board software and used directly.

The mean of each group of triplicate measures was used to compare analogous values from each device in a pair-wise fashion via Bland-Altman plots [24]. Paired t-tests by generalized estimating equations to account for multiple imaged eyes per person were used to identify any significant differences from zero (with $\alpha = 0.05$) between the SDOCT measures and reference values. Agreement between devices was determined by calculating pair-wise intraclass correlation coefficients (ICC). A bootstrapping type of resampling method was used to determine ICC to account for multiple imaged eyes from the same subject [25]. The standard deviation of the triplicate measures on each device was used to indicate the variability of intra-device measurements.

3. Results

3.1. Phantom imaging

The 3 topography calibration spheres had manufacturer listed radii of curvature of 6.15 mm, 8.00 mm, and 9.65 mm. The measured SDOCT values were 6.19 mm, 8.02 mm, and 9.69 mm. The mean of the paired differences in radii was 0.032 mm with a p-value by Wilcoxon signed rank testing of 0.25.

The 6 rigid gas permeable contact lenses had manufacturer specified base curves of 7.30 mm, 7.50 mm, 7.60 mm, 7.70 mm, 7.80 mm, and 8.20 mm. The manufacturer tolerance for the base curves was ±0.02 mm. Table 1 shows the measured SDOCT values for each contact lens. The mean of the paired differences was 0.003 mm with a p-value by Wilcoxon signed rank test of 1.00.

Table 1. Mean of Triplicate Base Curve Measurements (in mm) by SDOCT in Contact Lens Phantoms[a]

SDOCT	7.31 ± 0.01	7.48 ± 0.003	7.60 ± 0.001	7.70 ± 0.003	7.80 ± 0.006	8.21 ± 0.006
Reference Value	7.30 ± 0.02	7.50 ± 0.02	7.60 ± 0.02	7.70 ± 0.02	7.80 ± 0.02	8.20 ± 0.02

[a]The standard deviations for the reference values refer to the manufacturer's specified tolerance.

Each contact lens also had a manufacturer specified central thickness of 130 µm ± 20 µm each. The mean measured SDOCT central thicknesses for each of the 6 contact lenses was 133.67 µm (±0.12 µm), 136.10 µm (±0.10 µm), 125.23 µm (±0.23 µm), 131.33 µm (±0.12 µm), 143.77 µm (±0.15 µm), and 140.83 µm (±0.15 µm).

3.2. Subject imaging

29 eyes from 15 healthy subjects (mean age 30.7 years old, range 22 to 47 years old) were imaged. 9 of the subjects wore refractive correction with a mean spherical equivalent spectacle correction of −5.65 D ± 3.48 D in that group of 9.

Three volumes from 3 eyes of 3 subjects were unable to be segmented by the automatic segmentation algorithm. These were discarded, so for those 3 eyes, there were only duplicate SDOCT measurements and not triplicate measurements as in the other 26 eyes included in this study.
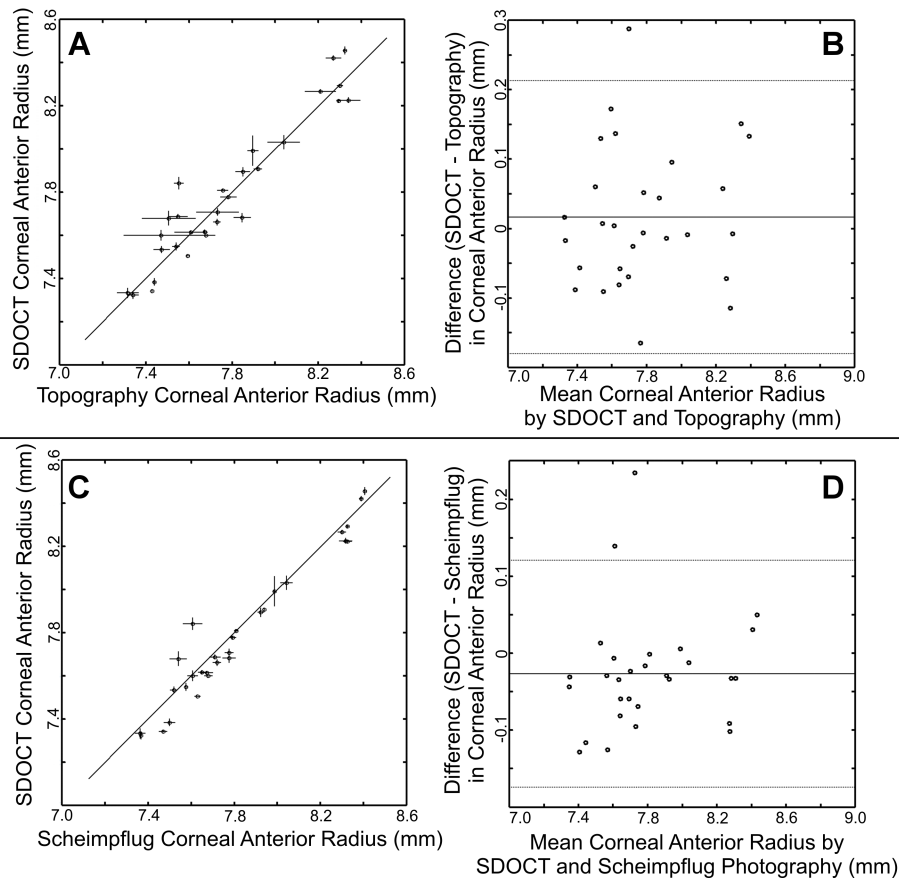

Fig. 2. **SDOCT measurements of corneal anterior radius compared to topography (A,B) and Scheimpflug photography (C,D).** For each comparison, the left figures (A,C) are direct plots of all the mean SDOCT measurements with all the mean measurements from the other modality. The vertical error bars represent ±1 standard deviation from the repeated SDOCT measures for that eye. The horizontal error bars represent ±1 standard deviation from the repeated other modality measures for that eye. The solid diagonal line represents the ideal 1:1 case. For the Bland-Altman plots on the right (B,D), the mean of the paired differences is represented by the solid line. The thinner lines above and below represent ±1.96 standard deviations from the mean of the paired differences. The SDOCT pairwise intraclass correlation coefficient to topography was 0.96 and to Scheimpflug photography was 0.98.

Data for corneal anterior radius measurements and corresponding Bland-Altman plots are shown in Fig. 2. The mean paired difference between SDOCT and topography (SDOCT-topography) was 0.016 mm ± 0.101 mm. This was not significantly different by paired t-testing with generalized estimating equations (p = 0.5025). The ICC by resampling method was 0.94 with lower and upper confidence limits of 0.88 to 1.00. For SDOCT and Scheimpflug photography (SDOCT-Scheimpflug photography), the mean paired difference in corneal anterior radius was −0.027 mm ± 0.075 mm. This was not significantly different by paired t-testing with generalized estimating equations (p = 0.1556). The ICC was 0.96 with lower and upper confidence limits of 0.91 to 1.00. For Scheimpflug photography and

topography (Scheimpflug photography-topography), the mean paired difference was 0.043 mm ± 0.048 mm. The ICC was 0.98 with lower and upper confidence limits of 0.95 to 1.00.
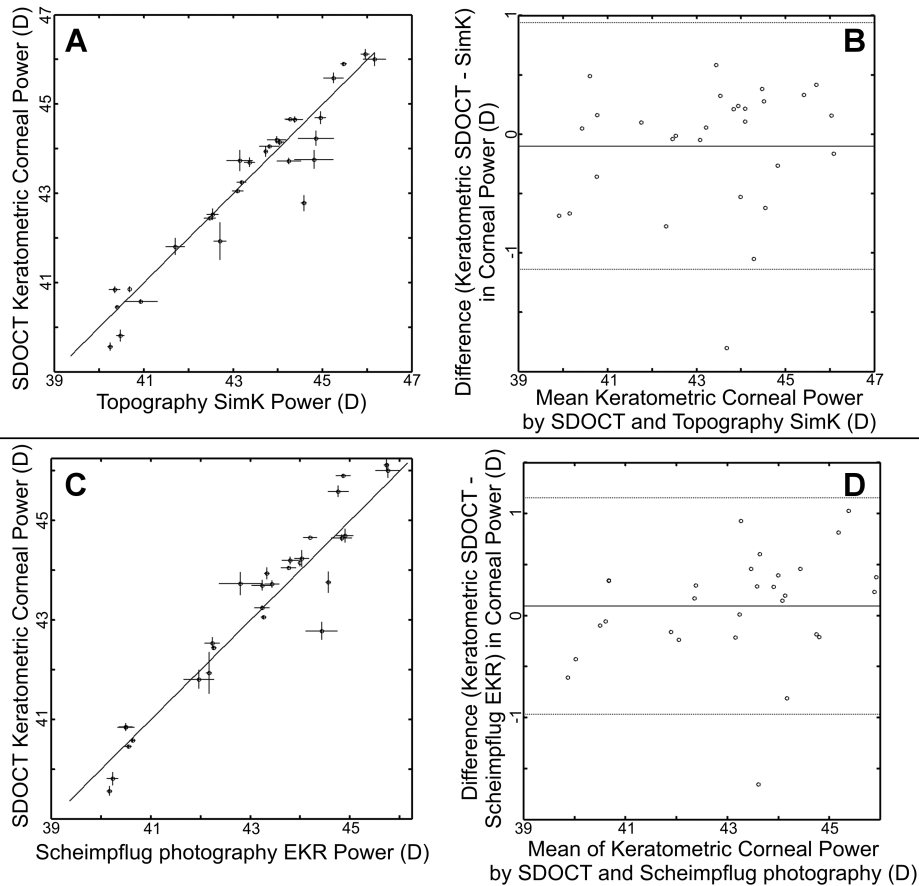

Fig. 3. **SDOCT measurements of keratometric equivalent power compared to topography SimK (A,B) and Scheimpflug photography EKR (C,D).** Similar to devices using 1.3375 as the keratometric index of refraction, keratometric equivalent power for SDOCT references the focal point to the posterior vertex (Eq. (3). For each comparison, the left figures (A,C) are direct plots of the mean SDOCT measurements with the mean measurements from the other modality. The vertical error bars represent ±1 standard deviation from the repeated SDOCT measures for that eye. The horizontal error bars represent ±1 standard deviation from the repeated other modality measures for that eye. The solid diagonal line represents the ideal 1:1 case. For the Bland-Altman plots on the right (B,D), the mean of the paired differences is represented by the solid line. The thinner lines above and below represent ±1.96 standard deviations from the mean of the paired differences. The SDOCT pairwise intraclass correlation coefficient to topography was 0.94 and to Scheimpflug photography was 0.98.

The mean paired difference between SDOCT paraxial corneal power (Φ) and topography SimK (SDOCT-topography) was −0.91 D ± 0.52 D. This was significantly different by paired t-testing with generalized estimating equations (p < 0.0001). The ICC by resampling method was 0.81 with lower and upper confidence limits of 0.64 to 0.98. For SDOCT and Scheimpflug photography EKR (SDOCT-Scheimpflug photography), the mean paired difference in corneal power was −0.71 D ± 0.52 D. This was significantly different by paired t-testing with generalized estimating equations (p < 0.0001). The ICC was 0.85 with lower and upper confidence limits of 0.71 to 1.00.

Figure 3 shows the data and corresponding Bland-Altman plots when SDOCT keratometric equivalent power (as defined by Eq. (3) in the Methods) is used for comparison.

The mean paired difference between SDOCT keratometric equivalent power (ΦKEP) and topography SimK (SDOCT-topography) was −0.10 D ± 0.53 D. This was not significantly different by paired t-testing with generalized estimating equations (p = 0.43). The ICC by resampling method was 0.95 with lower and upper confidence limits of 0.88 to 1.00. For SDOCT and Scheimpflug photography EKR (SDOCT-Scheimpflug photography), the mean paired difference was 0.09 D ± 0.54 D. This was not significantly different by paired t-testing with generalized estimating equations (p = 0.48). The ICC was 0.94 with lower and upper confidence limits of 0.88 to 1.00. For Scheimpflug photography EKR and topography SimK (topography-Scheimpflug photography), the mean paired difference was 0.19 D ± 0.29 D. The ICC was 0.98 with lower and upper confidence limits of 0.95 to 1.00.

Topography is unable to measure posterior corneal radii or central corneal thickness, so for those two biometric measurements, only a comparison between SDOCT and Scheimpflug photography was made. The mean paired difference between SDOCT and Scheimpflug photography measurements of posterior corneal radii (Scheimpflug photography—SDOCT) was 0.180 mm ± 0.076 mm; this was significantly different by paired t-testing with generalized estimating equations (p < 0.0001). The mean standard deviation of repeated posterior corneal radii SDOCT measurements was 0.028 mm (range 0.003 mm to 0.113 mm). The mean standard deviation of repeated posterior corneal radii measurements with Scheimpflug photography was 0.040 mm (range 0.006 mm to 0.121 mm). The ICC by resampling method was 0.74 with lower and upper confidence limits of 0.50 to 0.99.

For central corneal thickness, the mean difference between SDOCT and Scheimpflug measurements (Scheimpflug photography-SDOCT) was 21.27 μm ± 8.72 μm; this was significantly different by paired t-testing with generalized estimating equations (p < 0.0001). The mean standard deviation of repeated central corneal thickness measurements with SDOCT was 1.99 μm (range 0.148 μm to 7.934 μm) and with Scheimpflug photography was 4.21 μm (range 0 μm to 19.655 μm). The ICC by resampling method was 0.71 with lower and upper confidence limits of 0.53 to 0.88.

Figure 4 summarizes the standard deviation of repeated measures to demonstrate the measurement variability for keratometric power and corneal anterior radius, and Fig. 5 summarizes the relationships between the studied imaging devices for the same measures.

A. topography

± **0.167 D** (0.00 to 0.4375)
± **0.0416 mm** (0.00 to 0.173)

B. SDOCT

± **0.112 D** (0.0099 to 0.421)
± **0.0169 mm** (0.0001 to 0.0697)

C. Scheimpflug photography

± **0.149 D** (0.00 to 0.436)
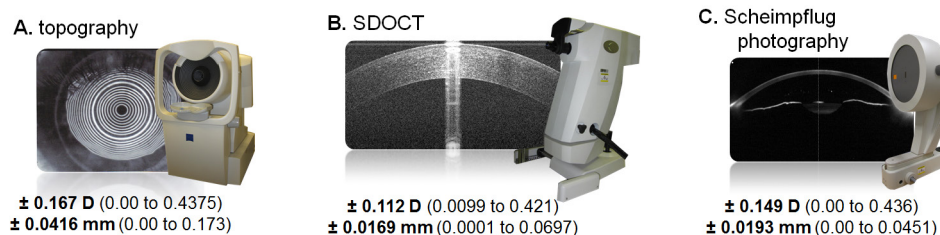± **0.0193 mm** (0.00 to 0.0451)

Fig. 4. **Variability of Repeated Measures.** Variability here is the standard deviation for a group of triplicate measures (except for 3 eyes which were duplicate measures). The bold face number is the mean of the standard deviations of repeated measures with the associated range shown in parentheses. The keratometric power (SimK for topography, keratometric equivalent power for SDOCT, and EKR for Scheimpflug photography) is listed first and then the anterior radius below it. Pooled standard deviations have been used in other works to describe repeatability. For comparison, the repeatability of SDOCT keratometric power in our population as expressed by pooled standard deviation is 0.14 D.
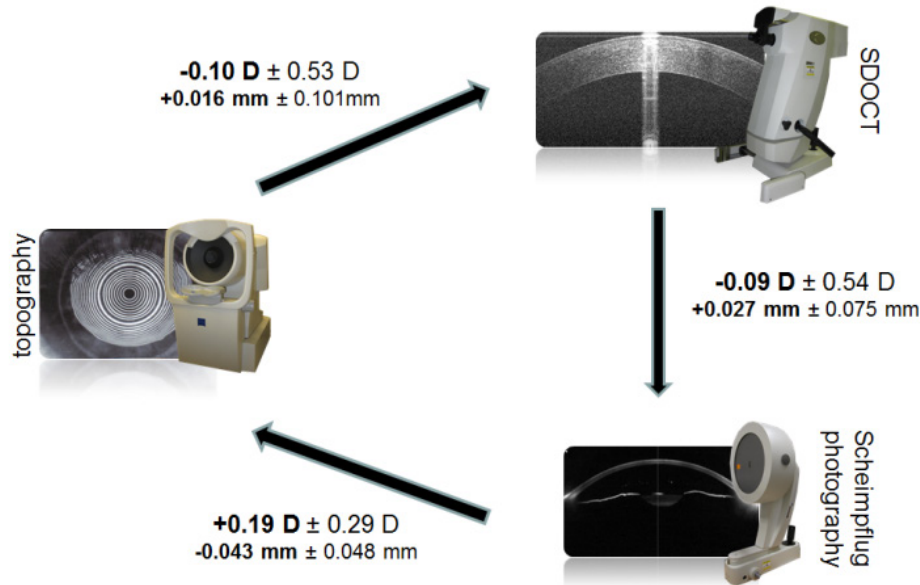
Fig. 5. **Differences between keratometric measures.** (left: topography, top right: SDOCT, bottom right: Scheimpflug photography.) The bold numbers are the mean paired differences between the devices connected by the arrows with the standard deviation of the paired differences. The sign corresponds to the direction of the arrow. The keratometric power is listed on top with the corneal anterior radius below.

4. Discussion

In this study, we have described a process to acquire relatively dense corneal tomographic volumes with a clinically available SDOCT system and to generate clinically useful corneal biometric measures. We then tested this process on phantom samples (calibration spheres and rigid gas permeable contacts lenses) and found that the SDOCT derived measurements did not differ significantly from the expected reference values. This demonstrated the validity of the process under controlled conditions.

We proceeded to apply this process to the clinical setting in normal eyes which allowed for the comparison of the SDOCT derived measures to those from existing clinical devices; using normal eyes allows the existing clinical devices to serve as reliable "gold standards" for comparison. Here we found that SDOCT measures of corneal anterior radius and keratometric equivalent power were in good agreement with topography and Scheimpflug photography. However, SDOCT derived paraxial corneal power was significantly different from topographic SimK values and Scheimpflug photography EKR values. Additionally, there was not good agreement between Scheimpflug photography derived corneal posterior radius and central thickness values using our process.

Addressing first the differences in paraxial corneal power, topography uses an artificial keratometric refractive index (typically $n_k = 1.3375$) to convert the only measured value—anterior corneal curvature—to a "power" value via $P = (n_k - n_{air})/r_a$. There are two assumptions inherent to the use of n_k. First, with Gullstrand model eye parameters, n_k only equals 1.3375 when the vertex power is used [22]. If the standard paraxial optical power from the thick lens formula is used, n_k would equal 1.3315 [1]. The difference in power (paraxial versus vertex) has an approximate effect of 0.8 D with Gullstrand model eye values and explains a large amount of the differences seen when comparing paraxial corneal powers to keratometric corneal powers in our study and others [12,26]. Using a SDOCT keratometric equivalent power based on the vertex power instead of the paraxial power largely eliminated the differences in power between SDOCT and the other two devices in our study.

The second assumption when n_k is used is that the posterior corneal curvature is related to the anterior curvature via a fixed ratio (usually r_p:r_a = 0.88 based on the Gullstrand model eye values of r_a = 7.7 mm and r_p = 6.8 mm). In post-refractive surgery eyes, this ratio is typically altered, but because we chose to study a normal population, we expected this ratio to hold. Further analysis of our data shows that our SDOCT r_p:r_a was 0.85 ± 0.013. The expected effect of this difference on corneal power using Gullstrand model eye values is approximately 0.2 D which is only slightly higher than the standard deviation of repeated measures for the devices used in our study.

The Scheimpflug photography r_p:r_a in our study population was 0.82 ± 0.010. This is similar to other studies utilizing the Pentacam which found the r_p:r_a ratio in normal eyes to be 0.82 ± 0.02 [27,28]. Utilizing this ratio, the expected effect on corneal power from Gullstrand model eye values is approximately 0.45 D. This effect, however, was not seen when comparing Pentacam EKR to topography SimK or SDOCT keratometric equivalent power (Fig. 5). This is likely because the algorithm used to generate EKR reportedly utilizes n_k within its calculation and effectively benchmarks itself to the keratometric power, negating the expected theoretical change [28].

Because the measured r_a values are similar in Scheimpflug photography and SDOCT in this study, the source of the r_p:r_a difference is in the significant difference between measured r_p. Our phantom data suggests that our SDOCT processing accurately recovers posterior curvature values with little variability, but this was under ideal conditions and not the clinical setting. If we assume that all devices can measure r_a similarly, we can use clinical r_p:r_a ratios in the literature to approximate the comparison of r_p values. In the literature, clinical r_p:r_a values range from 0.81 to 0.82 (Scheimpflug photography, Purkinje imagery) [29,30] to 0.84-0.85 (slitlamp photography, photokeratoscopy and pachymetry) [31,32]. In another study using SDOCT, the r_p:r_a ratio was found to be 0.84 [12]. Our ratio of 0.85 is within this range but on the higher end; the differences seen in these ratios are likely dependent on the techniques and methods used to remove optical artifacts from the imaged surfaces.

In addition to the posterior radii difference, SDOCT by our process also produces a central corneal thickness that is significantly different from Scheimpflug photography. Other comparisons of Scheimpflug photography and OCT measures of corneal thickness have shown variable outcomes with OCT lower in some [33,34] as in our study but equal in others [35,36]. In stationary phantom test objects with fixed indices, our process did recover the expected reference values with little variability in repeated measures for central thickness. We were unable to find the specified optical or pixel resolution of the Pentacam, but grossly viewing the output images, the Pentacam appears to have a lower optical resolution, both axial and transverse, than that of SDOCT. Clinically, our variability in repeated measures for the same biometric measures using SDOCT was also lower than that for Scheimpflug photography. There are likely additional differences between the imaging platforms in post-processing that may have contributed to the observed differences.

Motion errors are inevitable with any sequentially scanning imaging platform. While we performed rudimentary axial motion correction in this study, we did not address lateral motion. In previous work, we found that corneal power measurement was less sensitive to lateral motion than axial motion [16], but fully compensating for both axial and lateral motion would likely improve the accuracy of the imaged data and downstream measurements.

Faster scanning to reduce total scan time would also reduce potential corruption by motion. This was seen in the transition from slower TDOCT to faster SDOCT using 8 B-scan acquisition patterns. While the 8 B-scan pattern is acquired in only hundreds of milliseconds, the linear distance between adjacent 6 mm B-scans is up to 10% of the corneal diameter (1.17 mm) at the periphery of the scan. By using 50 6 mm B-scans in our study, the maximum linear distance between scans drops by an order of magnitude to 0.189 mm; this theoretically should produce a more comprehensive representation of the cornea. Despite our increased scan time, we were still able to recover anterior corneal curvatures that corresponded with

existing clinical measures. In addition, if we express repeatability as pooled standard deviations to allow for direct comparison, our dense 50 B-scan volumes had a repeatability of 0.14 D which is comparable to that of the faster, less densely sampled corneal SDOCT patterns in a previous study (0.19 D) [12].

By utilizing a dense scanning protocol, our OCT derived surfaces could also potentially be used directly in non-paraxial applications such as ray tracing. However, as our quantitative results only examined spherically fitted radii and derived power as is used in clinical biometry, we cannot yet comment on the accuracy of higher frequency spatial information in the extracted surfaces. Recent work by Ortiz et al. examining the surface elevations compared to reference modalities in a small series showed qualitatively comparable results, though there were differences in aspheric descriptors [37]. Should the higher frequency information be found to be more sensitive to motion artifacts, next-generation research SSOCT systems could mitigate motion artifacts by increasing imaging speeds while still retaining dense scan patterns [14,38]. Also, despite the good repeatability and correlation with SDOCT, the standard deviations of the differences between SDOCT and the other devices are high. This variability may be due to unresolved motion errors which could be reduced with increased imaging speeds.

We did not account for discrepancies between imaging system axis, ocular "optical" axis, and visual axis [21] other than asking subjects to fixate on a fixation spot coaxial with the system optical axis. Due to the limited imaging depth field of view in current-generation commercial SDOCT systems, we were unable to simultaneously image other ocular structures (iris, pupil) that would otherwise be helpful to locate those axes. Introducing a second camera, customizing the spectrometer for extended scan depth at the expense of resolution [39], or implementing complex conjugate artifact removal [40–43] are alternative customized strategies for imaging the deeper structures required for axis determination. Regardless, the spherical radii of curvature currently used clinically and in this study are only low pass filtered representations of the surfaces. We estimated the effect of an average disparity in axes [44] with spherical fitting would alter our power values by only 0.07 D [16].

5. Conclusion

We have demonstrated the accurate recovery of curvature values in phantom objects with dense, volumetric SDOCT scans. Clinically, the same acquisition process was then applied to normal corneas which showed good agreement of SDOCT measured anterior corneal radius and keratometric equivalent corneal power with existing clinical corneal biometric devices. The process described in this work for recovery of corneal biometric values from SDOCT for clinical use is broadly applicable to any currently available clinical SDOCT system with adequate characterization of the sample space.

Acknowledgments